Inflatable Aerodynamic Decelerator design for Spent Stage Recovery

Research · December 2021

DOI: 10.13140/RG.2.2.12691.81440

6 authors, including:

Alok Ranjan
Indian Institute of Space Science and Technology
1 PUBLICATION **0** CITATIONS
SEE PROFILE

Jay Rathod
Indian Institute of Space Science and Technology
2 PUBLICATIONS **0** CITATIONS
SEE PROFILE

Subrahmanya V. Bhide
California Institute of Technology
6 PUBLICATIONS **2** CITATIONS
SEE PROFILE

Harshit Vats
Indian Institute of Space Science and Technology
1 PUBLICATION **0** CITATIONS
SEE PROFILE

Research Paper

IAD design for Spent Stage Recovery

Alok Ranjan[1], Himanshu N[1], Jay Rathod[1], Subrahmanya V Bhide[1], Harshit Vats[1], and Deshmukh Vinay Vivek[1]

[1]Aerospace Department, Indian Institute of Space Science and Technology, Thiruvananthapuram

December 12, 2021

Abstract

This paper is a detailed summary of IAD based recovery for spent stage of a rocket. Initially three IAD designs were selected for study, based on literature, and one shape was selected by carrying out comparative CFD simulations. For the recovery the possibilities of usage of Grid fins, different materials for the IAD, Pressurization systems, parachute system and landing legs are studied. Finally CFD simulations are carried out for shape optimization and based on this trajectory is worked out keeping in mind the specifications for the smooth and comfortable landing.

Introduction

The history of Reusable Launch Vehicles dates back to the 1970s when NASA developed the partially reusable Space Shuttle which had a lifespan of nearly 30 years. The motivation came from the aircraft industry and also the high cost of access to space. Since then multi-stage expendable launch vehicles have been the primary approach to place payloads in orbit. Although being a reliable approach, the high cost of launch is a challenge yet to be addressed. Scientists attempt to design a fully reusable launch vehicle which reduces the cost of launch and to increase the launch rates.

Without compromising on the quality of material and resources, ISRO has been churning out successful missions despite limited budgets. Of course, ISRO has an advantage over NASA and other international space agencies in terms of low manpower costs and infrastructure running costs. "The cost of manpower that includes the salaries of the scientists and the cost of making a satellite and a spacecraft is much lower in India when compared to western countries. Most of the requirements are also outsourced to local manufacturers who provide finished material to ISRO to build satellites at less than half the price when compared to their foreign counterparts"(3). A system can be designed to recover a complete launch vehicle, separate stages or other components while making access to space economical. In order to decide which components to recover for reuse, it is important to understand the relative value of different launch vehicle components that are candidates for recovery and reuse, while minimizing the cost of recovery.

Recovery requires atmospheric reentry, deceleration, and landing. Reentry of the first stage of PSLV can be accomplished either via retro-propulsion, mid-air recovery, aeroshell, IAD or landing impact attenuation. Realising the future need for a system which ensures recovery, without compromising much of scientific payload, is realisable and scalable for heavier payload recovery, IAD is chosen over other competitors as subject for further study. An IAD in simple terms is an inflatable device which when inflated or deployed provides sufficient drag to slow down the body attached to it and ensure a safe landing. It is better than a parachute as it avoids the excessive oscillations at supersonic speeds. There is no standard shape for an IAD, however axisymmetric shapes are prevalent in available literature.

Mission Objectives

Our problem statement is as follows 'To study analyse and design an IAD based recovery sys-

tem for PSLV Stage 1'. The following are the parameters related to the PS1 stage:

1. Stage weight at burnout - 30 Tonnes
2. Separation Altitude- 68.5km
3. Velocity - 1.8443 km/s
4. Dimensions - 2.8m Diameter and 20.3 m Length
5. Time of separation - 113 s

The mission flow for the recovery system is that, after the separation, we maneuver the spent stage suitably to facilitate the IAD inflation.
After this the IAD is inflated and we are targeting to achieve a velocity of about 5-10 m/s before touchdown which will happen using Landing Legs on a barge. Additionally if the velocity decrement is not enough since the PS1 stage is considerably heavy we also keep the option for addition of a parachute open and study the possibilities. We also intend to use Grid Fins during the descent to stabilize the system which is also studied in the course of this project. Some literature based survey and comparison for the material that can be used for an IAD are also studied. Also the pressurisation systems are studied and control loops for pressurization is designed.

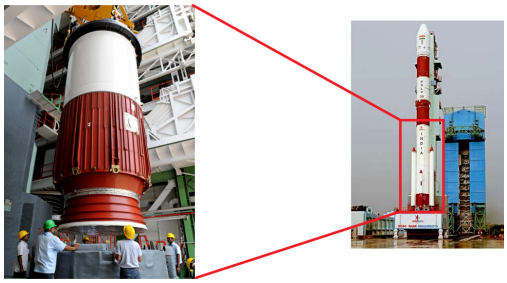

Figure 1: First stage of PSLV that we intend to recover

IAD Shape Selection

Generally, IAD designs can be divided into two categories.
Trailing IADs : In trailing IADs the decelerator is trailing the payload. The payload and IAD are usually attached by a towline or a group of towlines. Trailing IADs include sphere-shaped, teardrop-shaped, isotensoid shaped, torus and tension cone, etc.
Attached IADs : In attached IADs the decelerator is directly attached to the payload. This includes attached isotensoid, attached tension cone, stacked toroid blunted cone, etc. These types are shown in figure 2.

Figure 2: Different types of IADs (11)

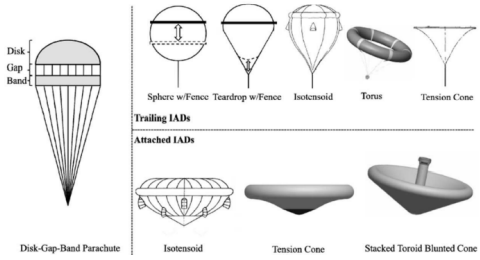

From these shapes the following 3 commonly used shapes were chosen for further analysis.

- **Trailing Ellipsoid**
  A trailing ellipsoid is a trailing type IAD. The IAD is connected to the payload using only one towline. The shape of the decelerator is ellipsoid i.e. any cross-section of this shape along the central axis will be an ellipse.
- **Attached Ellipsoid**
  The attached ellipsoid is similar to the trailing ellipsoid. But in this case, the IAD is directly attached to the payload.
- **Attached Tension Cone**
  The tension cone consists of two primary fabric components: a flexible shell that resists shape deformation by remaining under tension and an inflated torus. This torus sustains its internal pressure via a gas generator or pressure tank.

CFD analysis was done on these three shapes for different Mach numbers. After the analysis following results were obtained for Mach number 2.2

- Trailing ellipsoid : C_d=0.6939278
- Attached ellipsoid : C_d=0.6462677
- tension cone: C_d=0.631842

This analysis was done keeping the projected area (113.0973 m^2) and thickness(6.0012 m) of the IADs constant.
From this analysis, it was found that the trailing ellipsoid produced maximum drag values followed by attached ellipsoid and then the tension cone. But in determining the shape, drag is not the only factor. Other requirements are weight of IAD and complexity of vehicle integration mechanisms. A considerable part of this

weight will be due to the IAD integration mechanism. This includes an attachment, storage, deployment and inflation mechanisms.
Table 4 compares weight vectors of different mechanisms for different types of IADs. If this weight vector is high then it means that the weight will be lower.

Figure 3: Vehicle integration mechanism weight vectors(12)

Decelerator	Tension Cone	Attached Ellipsoid	Trailing Ellipsoid
Attachment Mechanism	0.017	0.015	0.04
Storage Mechanism	0.047	0.047	0.142
Deployment Mechanism	0.091	0.091	0.272
Inflation Mechanism	0.026	0.106	0.106
Overall Weight Vector	**0.182**	**0.259**	**0.559**

The ellipsoid decelerator, has a less complex inflation mechanism since an on board inflation system is not required. The attachment vector favoured the trailing ellipsoid mechanism. The attached type IADs require multiple attachment points, which increases overall complexity of that system. The deployment mechanisms favour the heritage hardware of the trailing ellipsoid. Trailing ellipsoid IAD has the highest overall weight vector. This means that the trailing ellipsoid shape will require less weight for vehicle integration. Hence, **the trailing ellipsoid was chosen as the shape for IAD**. Since, it produces more drag, requires less weight and has relatively simple mechanism for vehicle integration.

IAD's working

Inside Pressure

As soon as stage will get seperated from our launch vehicle and before it reaches very high speed heading toward earth, IAD will get inflated and a particular/required amount of gas will be injected for doing this so that $P_{inside} > P_{outside}$ but due to heat exchange with outer atmosphere P_{inside} may change with respect to height and we know $P_{outside}$ must increase rapidly as height decreases. So, by considering these factors before P_{inside} becomes $< P_{outside}$ we will again inject some moles of air inside our IAD to make $P_{inside} > P_{outside}$, and same thing can be repeated in more stages to make this process more effective and efficient.

Temperature variations

In the troposphere, the temperature generally decreases with altitude. The reason is that the troposphere's gases absorb very little of the incoming solar radiation. Instead, the ground absorbs this radiation and then heats the tropospheric air by conduction and convection. Since this heating is most effective near the ground, the temperature in the troposphere gradually decreases with increasing altitude until the tropopause is reached. This is the beginning of the stratosphere. In the stratosphere, the temperature remains isothermal until about 20 km. After that temperature actually begins to increase with altitude. From temperature of about -56.5C at 20 km, it increases to -2.5C at 50 km. The reason for this temperature fluctuation is that ozone absorbs the UVB (280-314 nm) radiation in the lower atmosphere. Higher in the atmosphere, however, normal diatomic oxygen absorbs the UVC (100-279 nm) radiation. Once it is absorbed, it is re-radiated at different wavelengths, thereby warming the stratosphere. At the top of the stratosphere (about 50 km, the stratopause), the temperature begins to decrease again as the altitude increases. Above the stratopause, in the mesosphere, thermosphere, and exosphere harmful gamma rays and X-rays are absorbed so temperature again increases.

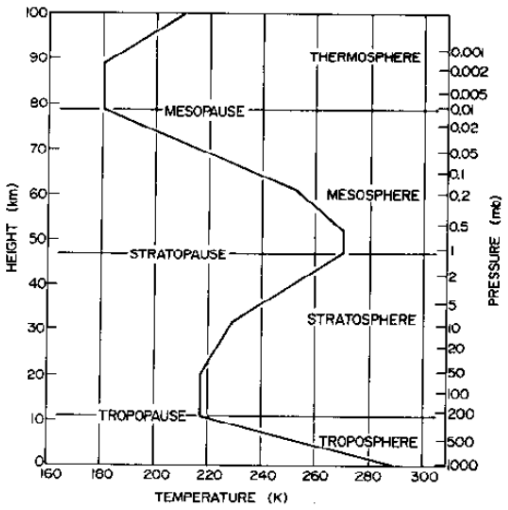

Car airbag system

Airbags work by inflating as soon as the vehicle starts to slow down as the result of an accident. They then begin to deflate as soon as the driver or passenger's head makes contact with them. If the airbag was not designed to deflate, then it would not solve the problem of the sudden

backward movement of the head and neck, as your head would simply bounce off it. All of this is possible because of a range of sensors and a small explosion. The airbag includes an accelerometer that detects changes in speed. If it detects deceleration above a preset speed, which is greater than normal braking speeds, it triggers the airbag circuit. The circuit passes an electrical current through a heating element, which in turn ignites a chemical explosive. This generates a large amount of harmless gas that rushes into a nylon bag. The bag, which is packed into a space behind the steering wheel or on the passenger side dash, inflates. When the driver or passenger's head makes contact with the bag, it begins to deflate with the gas escaping through small holes around the edges of the bag. By the time the vehicle has come to a full stop, the bag should have completely deflated. Similar process is being used in our IAD for inflation purpose i.e., injecting gas inside IAD to increase inside pressure. But instead of single stage our process will be in multiple stages.

Chemical Reactions Used to Generate the Gas

Gas-Generator Reaction	Reactants	Products
Initial Reaction Triggered by Sensor.	NaN_3	Na N_2 (g)
Second Reaction.	Na KNO_3	K_2O Na_2O N_2 (g)
Final Reaction.	K_2O Na_2O SiO_2	alkaline silicate (glass)

Table 1

This table summarizes the species involved in the chemical reactions in the gas generator of an airbag.

Note: Stoichiometric quantities are not shown.

Pressure controller

Figure. (4), shows a pressure controller which will help us to keep IAD's inside pressure more than outside by injecting extra required moles of gas inside IAD. After discussion and considering aerodynamics and structural factors we took a logical assumption i.e., $\Delta P = P_{inside} - P_{outside} = 0.25$. According to this design we proposed an active closed loop pressure controller which will take ΔP input from the pressure sensor and will run based on the conditions shown in figure. (4). By doing so we will be able to keep our IAD inflatted throughout its journey. In figure. (4), injector is a subsystem which will inject or remove gas inside IAD as instructed by the controller.

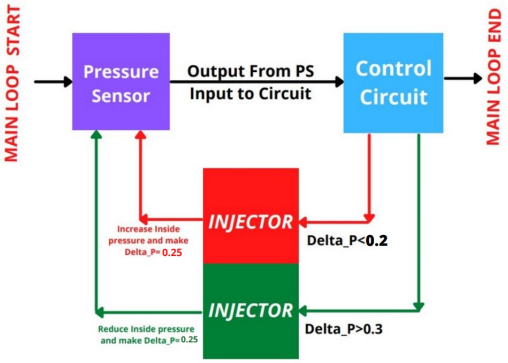

Figure 4: Closed loop pressure controller

Grid Fins

Grid fins are a type of flight control surface used in rockets and missiles. Grid fins have often been used on conventional missiles and bombs such as the *Vympel R-77* air-to-air missile; the *3M-54 Klub* family of cruise missiles. In 2014, SpaceX tested grid fins on a first-stage demonstration test vehicle of its reusable Falcon 9 rocket.

Guidance with grid fin is achieved by deflecting the fins from their original positions. Doing this, relative air flow changes its direction and aerodynamic lift force is generated. A grid fin rotates about its rotation axis, which is referred to as "hinge line", with the aid of an actuator motor aligned with the fin centerline. As a result, guidance commands coming into fin actuators create a rotational motion about the hinge line of each grid fin.

The flow field around lattice surfaces of a grid fin is classified by flight regimes which are distinguished with well-defined Mach number thresholds. Transonic flight with grid fins primarily suffers from high drag force. The reason for elevated drag is the internal flow field characteristics within the cube-like cells of grid fins. In the transonic regime, the flow inside the cells is choked and flow in upstream of the fins decelerates. This means that grid fins act as an obstacle to the flow so that drag force increases.

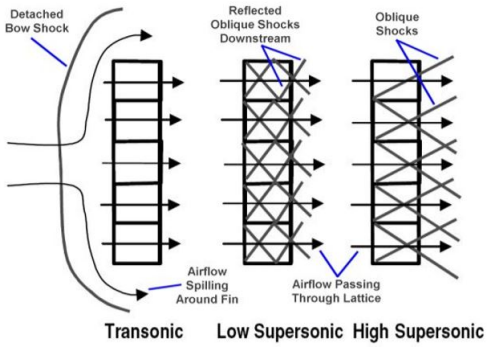

Figure 5: Flow patterns in different flight conditions

Primary advantage of using grid fins comes with significantly low magnitudes of hinge moment and minimal variation of center of pressure with changing flight conditions. On the other hand, grid fin is likely to be subject to high axial force for large number of lattice surfaces; however, it is possible to deal with this by careful web and frame design. Efforts on reducing the transonic drag penalty are becoming popular and this issue is currently being the main concern related to grid fin applications. Drag force on a grid fin at transonic speeds increases due to choking for Mach numbers below unity and shock reflections for those larger than unity. Locally swept grid fins, where sweeping is done for each individual cell, were validated as an effective tool for supersonic drag reduction, employing the sharp corners that diminish the strength of shock waves.

Geometric parameters

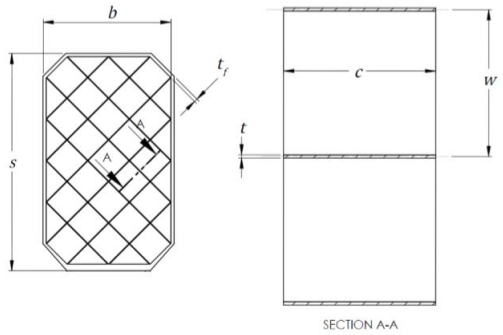

Figure 6: Grid fin geometric parameters

The above figure shows all the geometric parameters that results in a well-defined grid fin that has flat planform and blunt leading and trailing edges. Those parameters related to overall dimensions of grid fins are called as span (s) total width (b) and chord (c). The space occupied by the grid fin is driven by these three parameters. Width (w) and thickness (t) are those describing the dimensions of the individual cells. In addition to these, frame thickness (t_f), defines the dimension of the outer frame, which is can be utilized as the structural elements to keep the grid fins cell together.

The approximate relation between diameter (D) of the launch vehicle and the parameters defining grid fins geometry are :

$$s = 0.416D$$

$$b = 0.333D$$

$$c = 0.118D$$

Accordingly , for our case, span of the fins can be taken as **1.1667 m**, total width as **0.9324 m** and chord as **0.3304 m**

Behaviour of grid fins in different flight regimes

Use of grid fin in different flight regimes results in distinctive flow characteristics which usually determine the constraints of the design efforts. In general, Subsonic(M $<$ 0.7)and high supersonic (M $>$ 2.0) regimes are admitted as the best performance conditions for grid fins. Literature indicates that subsonic operation of grid fins is never seen as problematic because of absence of complex flow particular to this regime. Aerodynamic behavior of the grid fins is predictable with no special attention to flow field characteristics.

For the transonic flight, depending on the area ratio and free stream Mach number, it is possible to observe choking, when local Mach number at any region within the grid fin cell reaches to unity. For a specific Mach number, choking is observed below a certain 'critical area ratio'. This threshold can be calculated by the equation given below (air as the fluid) for any free stream Mach number.

$$\frac{A}{A^*} = \frac{1}{M_\infty}\left[\frac{5}{6}(1 + 0.2M_\infty^2)\right]^3 \qquad (1)$$

A grid fin in supersonic flight is exposed to shock waves in different patterns, depending on the Mach number of the flow. For the Mach numbers that are slightly larger than 1.0, a bow shock occurs in front of the leading edges of the grid fin. At a certain Mach number value shock waves become attached to leading edge. After this threshold, oblique shock and rarefaction waves are observed in case of any change in

direction of the air flow.

The grid fin flow regimes are separated by definite Mach number thresholds, called 'critical Mach numbers' (M_{cr1}, M_{cr2}, M_{cr3}).

Flow regime	**Lower bound (M_∞)**	**Upper bound (M_∞)**
Subsonic	0	M_{cr1}
Choked flow	M_{cr1}	1
Bow shock	1	M_{cr2}
Reflecting wave pattern	M_{cr2}	M_{cr3}
Non-reflecting wave pattern	M_{cr3}	∞

From literature, the approximate values of M_{cr1}, M_{cr2} and M_{cr3} are 0.8, 1.4 and 1.9 respectively. So, after all these studies it is clear that the grid fins should be used in the subsonic regions because it does not require any kind of shock formation, and shock formation can very much interfere with the whole body.

Fundamental consideration in design of a grid fin

Design procedure aims to arrange an effective configuration of grid fins in terms of aerodynamic stability and control. This is ensured by creating sufficient amount of moment about center of gravity of a missile. In this design process, longitudinal static stability and pitching moment control are of interest.

In general, the stability parameter, which is change in pitching moment coefficient with respect to angle of attack, C_{m_α}, has a negative value for stable missiles. The higher magnitude of this parameter, the stronger static stability. Logitudinal control of the stage is performed by means of pitching moment created by deflection of grid fin control surfaces. The change in pitching moment coefficient with respect to elevator angle, $C_{m_{\delta_e}}$, is linear in nature within a few degrees of rotation. By definition, positive deflection angle yields a positive moment.

Control characteristics is generally influenced by C_{m_α} and $C_{m_{\delta_e}}$ parameters. A new parameter, pitch control effectiveness, in introduced as $\frac{\alpha}{\delta_e} = \frac{C_{m_{\delta_e}}}{C_{m_\alpha}}$, which expresses, roughly, how much deflection angle is required to obtain a certain angle of attack value. According to literature, this value should be greater than 1.

Overall dimensions of the design should be taken as one of the considerations in evaluation of the design alternatives. Design efforts should also aim at a manufacturable, utilizable and maintainable solution.

Neglecting heat transfer and assuming constant geometry for the grid fins, we can determine few simple dimensionless parameters that influence the performance characteristics.

$$C_N = \frac{F_N}{0.5\rho v_\infty^2 L_\infty^2} = f_1(Re, M_\infty, \alpha, \delta)$$

$$C_A = \frac{F_A}{0.5\rho v_\infty^2 L_\infty^2} = f_2(Re, M_\infty, \alpha, \delta)$$

Since, grid fins is also used at the time of reentry of the first stage, therefore a material with very high heat resistance should be used in its manufacturing. Generally, **titanium** is used for this purpose. The mass of grid fins used in launch vehicles is approximately **30-40 Kg**.

Landing Subsystem

Study on Landing Leg Configurations

The major components involved in the landing subsystem are Legs and their energy absorbing capabilities. In general, the configuration of legs for landing, are classified into two :
1. Fixed Leg Configuration
2. Deployable Leg Configuration

Fixed Leg Configuration

As the name suggests, the fixed legs are attached to the body before liftoff, and remain attached throughout the flight duration. Usually, the number of legs attached are four and they are symmetrical. In figure 8, the overall scheme of fixed legs and schematic representation of damper is shown. The overall scheme consists of the retraction system and attenuation system. In which, piston and cylinder are involved in retracting, and hydraulic or honeycomb damper as well as foot pad is involved in attenuating. Typical bearings are used with pistons to complete the overall basic structure.

Fixed Leg Configuration

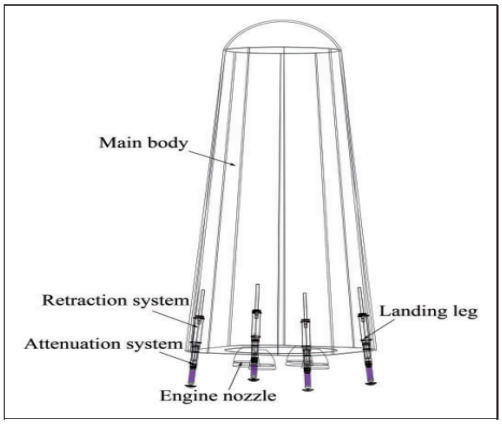

Figure 1. Overall scheme of vertical landing RLV.

(a)

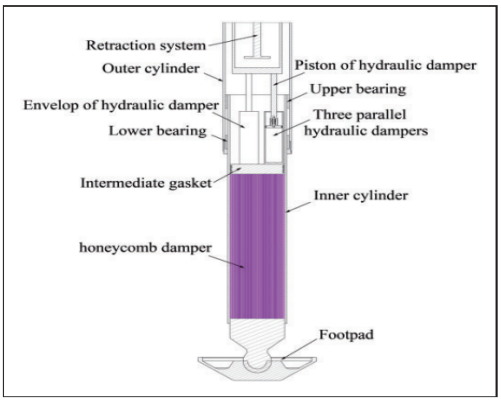

Figure 2. Schematic representation of oleo-honeycomb damper.

(b)

Figure 8: Fixed Leg Configuration

Deployable Leg Configuration

In contrast with the previous one, this configuration allows the legs to deploy out during the landing of the recovering stage. Mechanism of retracting and deploying the legs can be controlled. In figure 9, retracted and deployed state of overall scheme, as well as retraction profile and deployment profile of landing legs are shown. Usually, the auxiliary legs have constant length and the main landing legs have three stages of struts and lockers involved, as can be seen in figure 10.

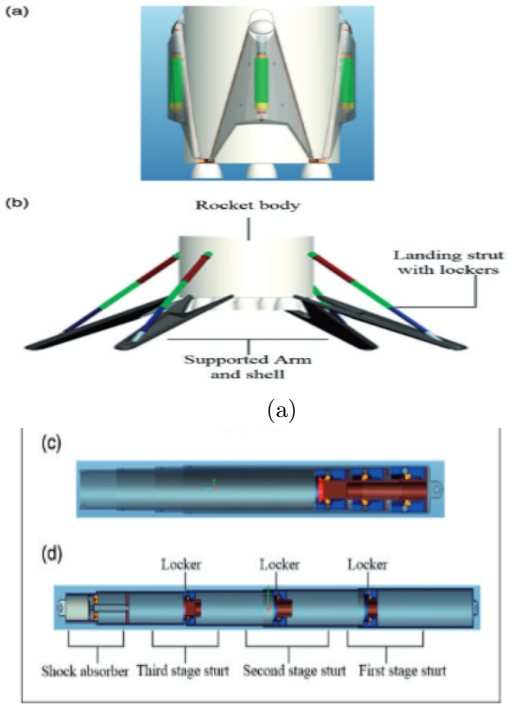

Figure 1. Landing gear's retraction and deployment: (a) retracted state; (b) deployed state; (c) retraction profile of landing strut; (d) deployment profile of landing strut.

(b)

Figure 9: Deployable Leg Configuration

Selection of Feasible Leg Configuration

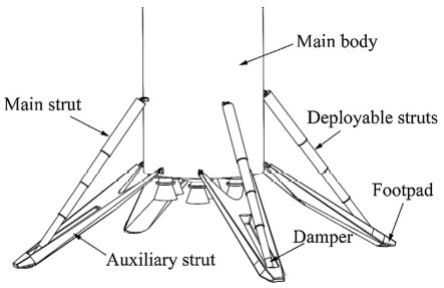

Fig. 1. Overall architecture of the considered landing gear system.

Figure 10: Chosen Deployable Leg Configuration

After the literature survey, the performance of fixed and deployable leg configuration, are found to be approximately equivalent for particular kind of recovering body. Hence, to choose a specific configuration, the following aspect can be emphasised. For the fixed leg configuration, the legs are attached to the body throughout the flight interval, due to which, during ascent, the legs can act as an extra drag creator and even can lead to shock formation, which catastrophes the whole objective of landing. Whereas, the use of deployable leg configuration do not affect the

flight in terms of extra drag creation, since the legs are well attached to the surface of the body and even are aerodynamically designed.

Therefore, the Deployable leg configuration is chosen for the landing purpose in this project, for which, the overall architecture is shown in figure 10, and corresponding analysis is performed in further sections.

Geometric Topological Model of Landing Legs

The overall scheme includes four landing legs symmetrically arranged. Each leg contains a retractable pillar with the absorber, an auxiliary shell, and a footpad. Among them, the retractable pillar is composed of a three-stage sleeve. During the launching, the sleeve is in a retracted state. The landing legs are wrapped and protected by an auxiliary shell closely attached to the surface of the vehicle body by a locking device. While ready for landing, the retractable pillars are elongated. The entire mechanism is unfolded around the auxiliary pillar hinge point, and the sleeves are locked by built-in locks when in place. The landing energy is absorbed by the dampers.

2D Topology with Coordinate System

A coordinate system called O-XYZ is shown in figure **??**. O at the center of the body's bottom surface. The positive direction of the OY axis is upward along the axial direction of the rocket body. The OX axis is located on the plane of symmetry of the vehicle whose positive direction points to the left. The landing legs are symmetrically distributed in the three dimensional space. Projecting the landing legs in the XY plane. The deploying and retracting two dimensional topology map of the left landing leg is shown in **??**, which shows three topological states of the legs in the release process before landing: Triangle ABE (State 1: the state of landing leg locked on the surface of the body), Line ABD (State 2: the state of the retractable pillar fully retracting) and Triangle ABC (State 3: the state of landing leg fully expanding).

L_{max}, L_{min} represent the maximum (State 3 (BC)), minimum length (State 2 (BD)) of a retractable pillar, L_r is the length of the retractable pillar when the landing leg is fully retracted (State 1 (BE)). Within the coordinate system O-XYZ, the coordinates of point A, point B, and point C can be given as (x_1, y_1, z_1), (x_2, y_2,0), and (x_3, y_3,0). The relationship of y1 and z1 can be expressed as:

$$y_1^2 + z_1^2 = R^2$$

where R is the radius of the vehicle body, which is 1400 mm.

According to the geometrical relation in the figure **??**, the length of the pillars in each state can be obtained as follows (14) :

$$L_{max} = \sqrt{(x_3 - x_2)^2 + (y_2 - y_3)^2}$$

$$L_a = \sqrt{(x_3 - x_1)^2 + (y_1 - y_3)^2}$$

$$L_{min} = L_a - \sqrt{(x_2 - x_1)^2 + (y_2 - y_1)^2}$$

$$L_r = \sqrt{\sqrt{(x_1 - x_2)^2 + (y_1 - y_2)^2} - L_a^2 + 2L_a\sqrt{(x_1 - x_2)^2 + (y_1 - y_2)^2}\cos(b)}$$

where,

$$b = \arcsin\left((x_2 - x_1)L_a\right)$$

$$\alpha = \arcsin\left(L_a \sin(b)\sqrt{(x_2 - x_1)^2 + (y_2 - y_1)^2}\right)$$

Simplification of Deployable Strut Model

To facilitate the analysis of the length of the retractable pillar, the pillar is simplified as follow: The length of each sleeve is equal and 'L'. Each lock is of the equal length L_1. The upper of the first stage sleeve is provided with a cap, and its length is L_0. The simplified model of the retractable pillar is shown in **??**, where L_d is the length of the damper.

The minimum and maximum length of the structure can be written as:

$$L_{kmin} = L_d + L + 2L_1 + L_0$$

$$L_{kmax} = L_d + 3L + L_0$$

To meet the requirements for deployment,

the minimum length of the structure should be less than or equal to the overall minimum required length, which can be denoted as:

$$L_{kmin} \leq L_{min}$$

The design margin of the retractable pillar length is defined as follows:

$$e = L_{min} - L_{kmin}$$

Mechanisms Involved

When the rocket is launched, the landing gear struts are in a retracted position, close to the rocket body, and do not affect the rocket launch. When the rocket lands, the strut is extended and locked to 135 °. The landing gear strut is composed of a rocket body, a new type three stages of struts of pneumatic extension mechanism with locking function, a shock absorber, a landing support with a rocker arm and fairing shell. The hydraulic shock absorber device is designed fixed with the third stage strut. The design principle is based on the compressibility of the fluids. Its basic components are an outer cylinder filled with liquid, a piston rod, and a valve or a special oil limit head. When the piston begins to move from zero load, the liquid is compressed by the piston rod which gradually occupies more volume. A valve is mounted on the piston rod to open during the compression of the fluid and to close to limit fluid flow when it is bounced. The seal of the outer cylinder is realized by the sealing of the inner wall of the outer cylinder and the piston rod. Mechanical Procedure of absorber can be given as follows:
the hydraulic absorber device is composed of a piston rod, a piston head, outer cylinders of damper,a sealing device, and a screw fastening device. As the landing struts contact the ground, the piston cylinder receives the counter force of the ground and moves upward. Then, the oil in the oil tank is compressed and moves to the oil chamber through the damping oil hole, and the damping force of the oil is generated. When the piston rod moves to the limit position in the outer cylinder, all the energy of the carrier is absorbed by the buffer. The energy stored behind the buffer forces the piston rod to move back and forth, and finally the carrier's attitude is restored.

Dynamic Equations for Hydraulic Absorber

The axial force of hydraulic absorber F consists of damping force of oil (f_h), oil spring force (f_a), internal friction force (f_f) and structural restriction (f_s).

$$F = f_h + f_a + f_f + f_s$$

where,

$$f_h = \begin{cases} \frac{\rho A_h^3 \dot{S}_a^2}{2C_d^2 A_+^2} & \dot{S}_a \geq 0 \\ -\frac{\rho A_h^3 \dot{S}_a^2}{2C_d^2 A_-^2} & \dot{S}_a < 0 \end{cases}$$

$$f_a = A_a \left[P_0 \left(\frac{V_0}{V_0 - A_a S_a} \right)^{\gamma} - P_{atm} \right]$$

$$f_f = \mu_m f_a \frac{\dot{S}}{|\dot{S}|} + \mu_b (|N_u| + |N_l|) \frac{\dot{S}}{|\dot{S}|}$$

$$f_s = \begin{cases} K_s.S & S < S_0 \\ 0 & S_0 \leq S < S_{max} \\ K_s.(S - S_{max}) & S \geq S_{max} \end{cases}$$

The interpretation of involved parameters are as follows : ρ is the density of the oil, A_h is the compressed oil area, A_+ is the orifice of the compression stroke, A_- is the orifice of the extension stroke, C_d is the coefficient of contraction, A_a is the area of compressed air, P_0 is the initial air pressure, V_0 is the initial air chamber volume, P_{atm} is the atmospheric pressure, and γ is the gas change index, S_a is the stroke of the piston. μ_b is the coulomb friction coefficient, N_u is the pressure generated by the upper support points of the piston rod and buffering strut, N_l is the pressure generated by the lower support points of the piston rod and buffering strut. S_0 is the initial stroke of the piston, S_{max} is the maximum stroke of the piston, and K_s is the contact stiffness between the piston and the envelope.

The damper is considered to have a single air cavity. When the external force pushes the damper, the oil in the chamber is squeezed into the gas cavity. The oil flows through one or more small holes, which dissipates energy in the form of heat energy. Meanwhile, part of the energy is stored by the compressed air.

Analysis

Geometric Parameters

The standard values of following parameters are considered from the literature : L_0 = 150 mm, L_1 = 180 mm, L_d = 550 mm. For simplification, values of some parameters are assumed such as e = 0, $L_{kmax} = L_{max}$, each of the three strut length to be L = 800 mm, distance between A and B to be 1000, distance between horizontal components of A and B to be 100 mm. These

values are considered by physical appearance of the overall structure. By Artificial Iterations of all the expressions described in section geometric topological model, the suitable geometric parameters are obtained as follows:
L_α = 2860 mm, L_{min} = 1860 mm, L_{max} = 3100 mm and α = 54.88 °. Hence, Auxiliary legs have constant length of 2860mm and main landing legs (which consists of three retractable struts) have length varying from 1860 mm to 3100 mm which takes the minimum value at α = 54.88 °.

Mass Evaluation : The dimensions of the main and auxiliary legs can be considered as 3100mm and 2860mm respectively, with mean diameter of around 0.3m and thickness of 0.02m, combination of all 4 legs results into volume of 0.2111 m^3 and with density of 2250 kg/m^3, leads to mass addition of around 475 kg to the overall system.

Feasibility Analysis

The following assumptions are considered : All the 4 legs touch simultaneously down. For a standard hydraulic absorber, the required parameters are taken from literature, such as, density of oil ρ = 960 kg/m^3, contraction coefficient c_d = 0.8, initial pressure P_0 = 1 MPa, etc. Energy conservation is carried out for transferring the overall kinetic energy of the system to compression capability of absorbers. Since, all legs are assumed to touchdown simultaneously, summation of axial forces experienced by the absorbers must be less than the impact force generated by landing. Let the horizontal velocity of the system at landing is 0.5 m/s with neglected pitch angles. Hence, for maximum allowed compression of 0.3 m for hydraulic absorber, the maximum allowed vertical touchdown velocity obtained is around 2 m/s.

Parachute and Material studies

A parachute is a flexible device who's primary purpose is to produce DRAG. The thin canopy material and slender suspension lines allow a big device to be packed in small volume. the purpose of the parachute is to create large drag area which in turn creates a large drag.

Types of Parachutes

- **Solid type canopy :** solid type canopy is fabricated mainly with cloth materials and it is relatively easy to made. these type of parachutes have no opening other than vent.

- **Slotted type canopy:** These Type of Parachutes with canopies fabricated from either cloth materials or ribbons. These types of parachutes have extensive openings through the canopy in addition to the vent. the slotted type canopy parachutes can be expensive to manufacture, these type of parachutes are most commonly used in planetary exploration missions.

Table 1: Parachute types and Cd ranges

Type of Parachute	Cd range
Disk gap band	0.52
Ring sail	0.75
Conical	0.75-0.9
Tri conical	0.8-0.89
Circular slotted	0.75-0.8
Aeroconical	0.635
Conical ribbon	0.5

Parachute system components

Recovery system involves more than one parachutes. The first thing to deploy is the drogue parachutes, the drogue parachute is designed to be strong so that it can withstand the high velocities in heavy loads of initial deployment. The drogue parachute provides some initial drag and stabilizes the system so that main parachute could come out from the packed device cleanly. The drogue parachute is attached to the main parachute bag with a long towline, The main canopy is inside the bag and it come out after 10 to 15 second after line is cut along the drogue to pull the main parachute bag out of the payload. The main canopy is designed to provide full deceleration of the payload and provides the soft landing of the system. The suspended line attached to the payload with weight, weight is transferred to the suspension line and suspension line transfer the load to the canopy.

Mathematical model for drag force

Drag and Weight act on the parachute as it falls through the atmosphere , when the parachute deploys, it creates more drag area, and produces more drag. According to 2^{nd} law of motion addition of more drag results in a lower acceleration. When a parachute of mass m is falling under the action of gravity, it is subjected to two distinct forces: weight mg, and the drag force, F_D.

Applying Newton's second law of motion in the vertical direction yields the following differential equation for the motion of the parachute:

$$m\frac{dV}{dt} + F_d - mg = 0 \tag{2}$$

$$F_d = \frac{1}{2}\rho V^2 C_D A_{ref} \tag{3}$$

where, V is the vertical speed, t is the time, and g is the acceleration of gravity.
When the body reach at equilibrium position, acceleration becomes zero.

$$DragForce = weight \quad \frac{1}{2}\rho V^2 C_D A_{ref} = mg \tag{4}$$

Selection of parachute and material

circular slotted parachute which we have chosen to use for our mission . From the paper(16) we found that the circular slotted parachute has less opening shock and also the minimum size for the same payload amongst the various parachutes. performance and drag coefficient between the circular slotted canopy and ringsail canopy are nearly same but Circular slotted parachute is easy to manufacture whereas ringsail requires high skill to maintain the sail dimension, bandgap, and porosity of the overall parachute. Nylon /kevlar hybrid material can be use for main parachute.

Parachute design

Main parachute design

In our project we are getting 400m/s at 5km altitude using the IAD, dynamic pressure will be around $58,864Pa$*, which is not feasible for open the parachute. If we can use any other method to reduce the velocity upto around 160m/s, then we can use the parachute system for recovery.*

`The calculation will be done for 160m/s velocity at 4km altitude`

The size of the cluster is determined by calculating the total effective drag area required.

$$q_e = \frac{1}{2}\rho(z)V^2, \rho(z) = \rho_0(1 - 22.57.10^{-6}Z)^{4.256} \tag{5}$$

Considering that in equilibrium descent the total drag of the system is very nearly equal to its weight, the required effective drag area can be obtained.

$$C_D S_0 = \frac{W}{q_e} \tag{6}$$

dynamic pressure at equilibrium for terminal velocity 20m/s at altitude $230m$ is $238pa$ $W = 30300kg$ so

$$(C_D S_0)_{1,2,3} = 415.88m^2$$

$$d_0 = \sqrt{\frac{4.S_0}{\pi}} = 26.57m$$

to get the terminal velocity 20m/s , diameter of the all three main parachute is 37.57m// percentage of drag loss is less than 5% for a cluster of three parachutes.

Opening force

For reefed parachute

$$D_f = \frac{\rho}{2} l_{fb} d_{fb} V^2 c_f s_f$$

$$D_f = 4039.4N$$

$$\ddot{x} = \frac{\Delta v}{\Delta t} = \frac{(117-31)}{234-220} = -6.1m/s^2$$

$$(C_D S_0)_R = \frac{2(m(g-\ddot{x})-D_f)}{\rho v^2} = 63.30m^2$$

$$(S)_0 = 84.4m^2$$

$$(D_0)_R = 10.36m$$

$$t_f = \frac{nD_0}{v}\left(\frac{(C_D S)_R}{C_D S)_0}\right)^{0.5} = 0.864second$$

$$F(X)_{reefed} = (C_D S)_R.q_R.C_X.(X_1)_R = 501579N$$

$$F(X)_{Disreefed} = (C_D S)_D.q_D.C_X.(X_1)_D = 163501N$$

Opening coefficient can be consider as $C_X = 1.05$, $(X_1)_R = 1$, $(X_1)_D = 0.4$

Material Selection for IAD and parachute

Materials that are used in the construction of an IAD must be flexible, lightweight, and strong. In addition, the materials must withstand tight folding, temperature extremes ultraviolet (UV) degradation, vibration, and other harmful environmental elements. There are many light-certified flexible materials are available. kevlar 29 is one of the good material that is used in many space missions.

Kevlar is an excellent material for primary load-carrying members such as suspension lines, and it reduces the parachute's weight and volume. The drawbacks of Kevlar are its loss in strength due to moisture absorption or smog storage environment; it is not as resistant to abrasion, and it is slightly more difficult to manufacture compared to nylon. Another drawback of Kevlar is its higher cost, about a factor of 3 greater than nylon. So we are using the nylon

hybrid material for IAD , because it is cost effective and exhibits good strength to weight ratio. Recovery using parachute is not feasible for our mission because it cannot open at high velocity. it can be operate when load velocity can be reduced by any other method like retro thruster. when it opens at high dynamic pressure it can break the IAD and suspension line, also if we use multiple cluster parachute then the weight of the system will increase.
From basic calculations the weight of the main canopy (nylon) is obtained as, $W_{canopy} = 0.0598(D_0)^{2.046} = 49kg, W_{3canopy} = 147kg \ \ approx$

Shape Optimization

Aerodynamic analysis is a vital element in the present study for the design of the IAD for spent-stage recovery. The main use of IAD is to decrease the peak dynamic pressure during descent. This is done by decelerating the stage in the upper atmosphere. For this the IAD should augment the drag of the stage sufficiently, but should not add significant mass to the system. A fixed aft mounted IAD has been proposed by ISRO for stage recovery studies. Another aspect is the study the stability characteristics of the stage. The configuration is expected to be stable because of the high drag producing IAD at the rear end. Hence, in the present study, the aim is to obtain the drag characteristics of the stage with trailing IAD and study the flow-field around the two bodies.

Extensive CFD simulations have been carried out to estimate the required drag. 2-D axisymmetric simulations are carried out for the purpose of characterization since the IAD and stage are axisymmetric. As the aerodynamic data generation is very compute and time intensive and is required for a very large number of configurations during the design optimization studies.

Mesh Generation

The very first step in CFD analysis is discretization, which involves splitting the domain of interest into smaller sub-domains and cells. This process of discretization is called Mesh generation or meshing. The current project utilises the Pointwise software for meshing. The mesh quality determines solution accuracy, rate of convergence and also time required for computation. A good mesh should ensure all the expected flow features are captured. The domain chosen for analysis is a square of size twenty times the IAD maximum diameter to ensure negligible upstream influence of body. Structured meshing is undertaken throughout the domain owing to the relatively less complex geometry, higher accuracy, better convergence and lower memory requirement. To ensure that all the flow features are captured appropriately, specially near the boundaries of the body, fine meshing (initial cell height of 1e-6m)is done within 0.05m of the body boundary to capture the resulting boundary layer. The mesh quality is maintained by ensuring that the area ratio is within 3.0 and equiangle skewness within 0.85. Figure (13), shows an overview of domain where c is the the distance of IAD from stage and a and b are the IAD geometry parameters.

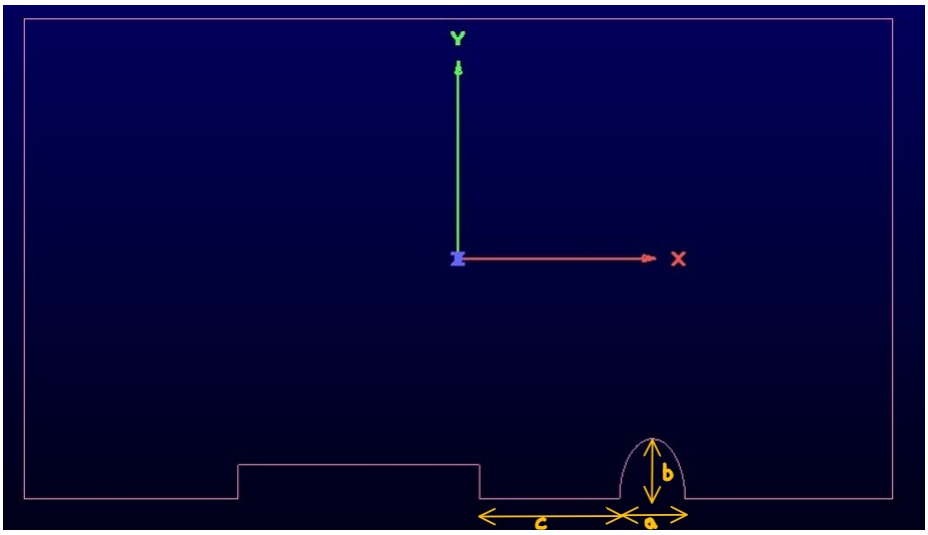

Figure 13: IAD geometric parameters

Computational results

We have tried varying our design parameter i.e., a, b and c at fixed mach number 3.2 and with respect to each other it was observed that increase in a was reducing drag while increase in b was contributing to increase net drag. While varying c it was observed that drag was first slowly increasing and suddenly reached a peak value and got saturated just near the peak value. Further, for trajectory design as required we had taken a reference height i.e., 25km and we have varied all three parameters individually and simulated with respect to different mach no.

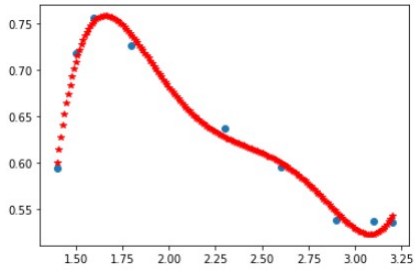

Figure 14: Cd vs Mach no. (a=5.5, b=5.8 and c=11.8)

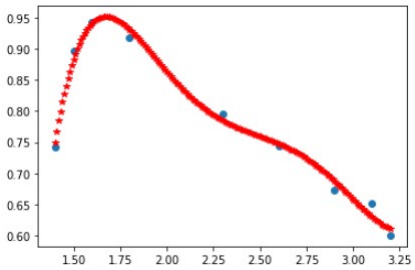

Figure 15: Cd vs Mach no. (a=5.5, b=7 and c=11.8)

Fig. (14) and (15), shows a set of results. In this way we have taken some set of outputs manually to feed into trajectory equations from where we were getting a feedback of requirement of drag and according to that we have varied design parameters keeping structural and stability factors in mind. For example, increase in b was giving us more drag which was a favorable thing but our stability of structure was reducing which was not in favour. Fig. (16) shows velocity profile for a simulation at 3.2 mach no. which clearly shows primary and secondary shock formations as well.

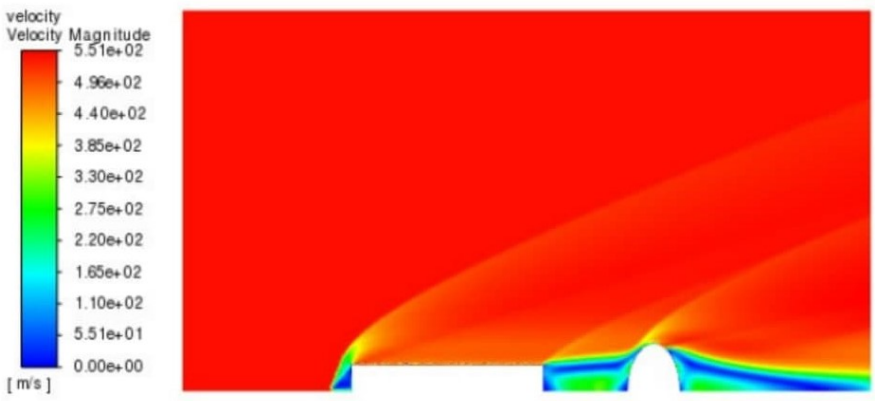

Figure 16: Velocity profile for a simulation at 3.2 mach no.

Trajectory Design

The main elements of the trajectory design work done are:

1. Trajectory Estimation without IAD
2. Thruster selection/design for pitch maneuver
3. Trajectory Estimation and Optimization with IAD

Governing Equations

We use the 3 kinematic equations and 3 dynamic equations to simulate the trajectory of the Spent Stage.

$$\dot{r} = vsin\gamma \tag{7}$$

$$\dot{\xi} = \frac{vcos\gamma cos\zeta}{rcos\phi} \tag{8}$$

$$\dot{\phi} = \frac{vcos\gamma cos\zeta}{r} \tag{9}$$

The equations 7, 8 and 9 are the kinematic equations.

$$\dot{v} = \frac{Fcos\alpha_T}{m} - \frac{\mu_E}{r^2}sin\gamma - \frac{D}{m} + \omega_E^2 r cos\phi(cos\phi sin\gamma - sin\phi cos\gamma sin\zeta) \tag{10}$$

$$\dot{\gamma} = \frac{Fsin\alpha_T}{mv} - \frac{\mu_E}{r^2 v}sin\gamma + \frac{v}{r}sin\gamma + \frac{L}{mv} + cos\phi(2\omega_E cos\zeta + \frac{\omega_E^2 r}{v}(cos\phi cos\gamma + sin\phi sin\gamma sin\zeta) \tag{11}$$

$$\dot{\zeta} = -\frac{v}{r}tan\phi cos\gamma cos\zeta + 2\omega_E cos\phi tan\gamma sin\zeta - \frac{\omega_E^2 r}{v cos\gamma}sin\phi cos\phi cos\zeta - 2\omega_E sin\phi. \tag{12}$$

The equations 10, 11 and 12 are the 3 dynamic equations. Here r is the distance from the center of the Earth, v is the velocity magnitude, ϕ is the lattitude, ξ is the longitude, *zeta* is the heading angle and γ is the flight path angle. The axis system for the above formulation is shwon in the Fig. 17.

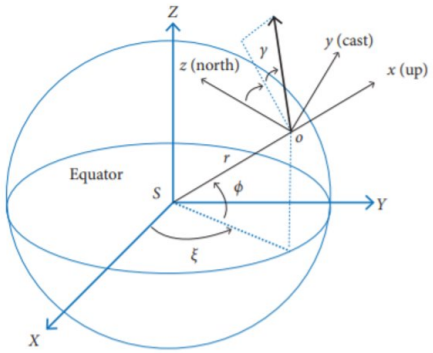

Figure 17: Planet-fixed and local horizon frames for atmospheric flight.

Since the Spent stage doesn't produce any Lift and also there is no Thrust produced, the two terms L and F can be made equal to zero. The Drag 'D' can be found by the expression 13.

$$D = C_D \frac{1}{2}\rho v^2 S_{ref} \tag{13}$$

The term ω_E is the angular speed of the Earth which is equal to 7.2925×10^{-5} rad/s. The term μ_E is the standard gravitational parameter for Earth which is equal to $3.986 \times 10^{14}\ m^3/s^2$. The term r is the sum of the altitude and the radius of earth taken to be 6378 km.

Trajectory Estimation without IAD

The Spent stage will follow a parabolic trajectory. This trajectory needs to be estimated initially so as to give us an initial idea regarding the timescale of the ascent so that suitable pitch maneuver can be designed.
This is done using the trajectory equations from the previous sections. The spent stage can be assumed to be a cylinder, the C_D for a cylinder in cross flow is known but in our case we require an initial estimate for the C_D for a cylinder with the flow along the axis of the cylinder. As an initial guess we we take the C_D values estimated for a fuselage which is almost similar to a cylinder but except the fact that the nose of the fuselage is aerodynamic but in our case it will be flat. Thus we conservatively estimate the C_D to be equal to 0.02. Using this in the trajectory equations we obtain the trajectory and velocity plots as shown in Fig. 18 and 19. (2)

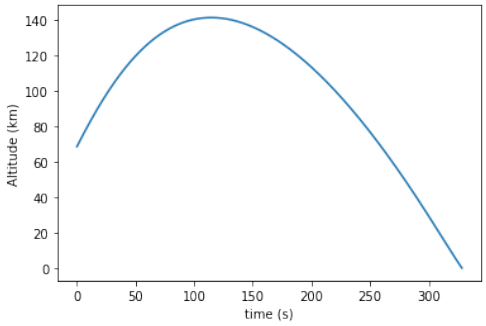

Figure 18: Trajectory estimate for the spent stage without IAD

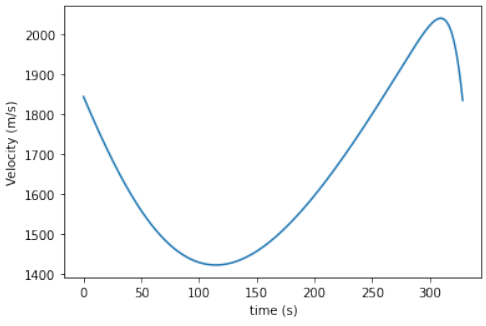

Figure 19: Velocity estimate for the spent stage without IAD

From the plots we can make the following observations,

1. The peak of the parabolic trajectory is attained after around 120s after separation.
2. The minimum velocity attained during this phase is around 1400 m/s.

Thus we have sufficient enough time for the pitch maneuver to be executed after which the IAD can be inflated at the top most point. This pitch maneuver and maintaining it as such is essential since the descent we require is vertical and only 1 IAD is used.

Thruster design for pitch maneuver

The pitch maneuver is essentially rotating the spent stage such that it becomes perpendicular to the local horizon. The pitch maneuver can be executed by using 4 cold gas/mono-propellant thursters. These thrusters provide thrust of the order of 10-100 mN using which the pitch maneuver can be executed in around 10-20 sec. The timing of this maneuver can be either of the three following options,

1. After the separation occurs (0-40 secs)
2. Somewhere in between (40 - 180 secs)
3. Just before the maximum height is reached (80 -100secs)

If the maneuver is done just after separation or somewhere in between, then for a considerable amount of time the velocity direction and orientation won't be aligned and thus would cause moments on the stage. Hence a better option is to execute the maneuver just before the top most point so that after the maneuver the IAD can be inflated.
This maneuver would involve firing of thrusters to make the spent stage vertical and thus suitable for inflating the IAD. Small Cold gas / mono propellant thrusters can be considered for this purpose.
In a general understanding Cold gas propellant systems are much simpler and less complex than mono-propellant systems. But along with this Cold gas systems have lesser specific impulses too. The variation of propulsion system mass and Total impulse is given in Fig. 20. From the figure it is evident that for lower total impulses required cold gas propellant system have lower mass than mono-propellant system. But at higher total impulse Mono-propellant would have lesser system mass

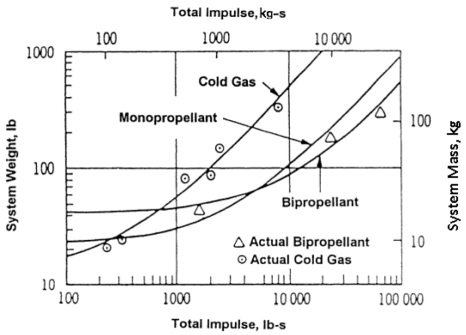

Figure 20: variation of propulsion system mass and Total impulse

Cold gas propellants mostly have Specific impulse lesser than 100 s, where as for mono-propellant systems hydrazine can provide a specific impulse of about 230 s. A mono-propellant system would require some additional components if it is a pressurised system. If it is a blow-down system then the mass and complexity of the mono-propellant would almost be the same as that of the cold gas system. Before finalizing the propellant system type we would want to have an idea of the range of thrust required for the maneuver. For this we solve the two point boundary optimization problem. We know the initial pitch angle of the spent stage and assuming a angular rate of zero, we need to reach the final point of 90 degree with the horizontal and zero angular speed. The thrust that we apply is the input and this has to be minimized. Employing the fmincon of MATLAB to minimize thrust given the boundary conditions we arrive at a linear thrust profile that would be required. The initial angle is around 45° considering some disturbance we assume the initial angle to be 40°. If the maneuver has to be completed within 14 secs we would require a maximum thrust value of 0.8N. This can be seen from the Fig. 21 and 22. For the worst case scenario if the IAD has to be turned from −90 to 90 we would require a thrust of 2.9N. This can be seen form the Figs. 23 and 24.

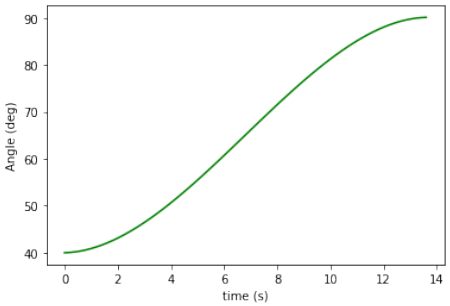

Figure 21: The variation of Angle with time for the pitch maneuver

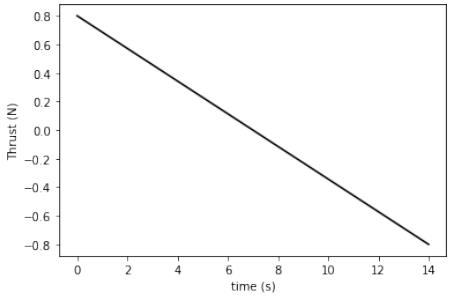

Figure 22: The variation of Thrust with time for the pitch maneuver

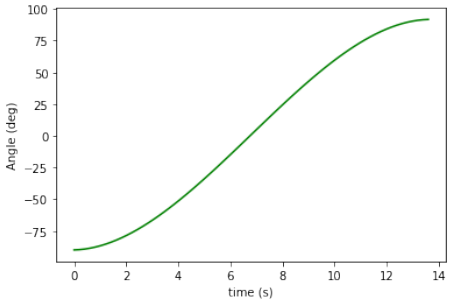

Figure 23: The variation of Angle with time for the pitch maneuver in the worst case scenario

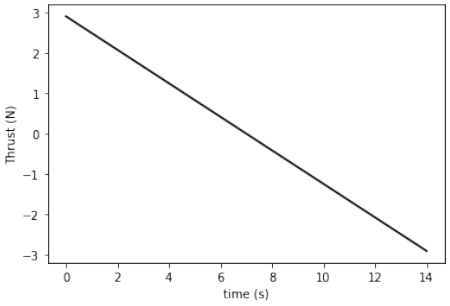

Figure 24: The variation of Thrust with time for the pitch maneuver for the worst case scenario

Therefore now we search for cold gas and mono-propellant systems which can provide thrust is similar range that is in the order of 1N to 5N and compare their properties. We will compare the MOOG MONOARC-5 and MOOG GN_2 058-118 cold gas propellants. A comparison table made 3. From the table we can see that in terms of mass, dimensions Cold gas propellant has an upper hand but it requires more power to operate than the mono-propellant system.

Table 3: Comparison of Cold Gas and Mono-propellant system

Property	Cold Gas System	Mono-propellant system
Nominal thrust (N)	3.6	4.5
Specific Impulse (s)	57	226
Power	30	18W
Mass	23g	490g
Dimensions	6.6 mm, 25.4 mm	41.8 cm, 2.5 cm

Considering the fact that PSLV is a working LV and the recovery system must cause as less payload penalty as possible it will be better to chose for the cold gas system rather than the heavier mono-propellant system. Also we would require control systems to control the Thrust in the fashion as shown in Fig. 22. (1) (9) (10).

Finally we can conclude this section by providing a mass approximate that is incurred due to the propulsion system. For the cold gas thrutser we have chosen, the thrusters have a mass of 23g and we use 4 thrusters thus we would have 92g.

Trajectory Estimation and Optimization with IAD

We now employ the trajectory equations and integrate them using odeint of the Scipy module which is a wrapper for the Runge-Kutta methods. The top most point is our start point and for the integration and is terminated once we reach the ground. For specific shape of the IAD the variation of Cd with Mach number is obtained from the IAD shape optimization studies and later they are employed to obtain the trajectory.

First Iteration

For the first iteration IAD shape and design the variation of Altitude and Velocity is shown in Fig. 25. This corresponds to the variation of Cd as shown in Fig. 14

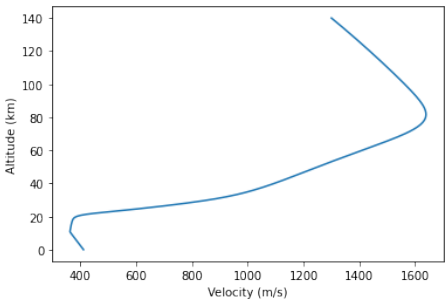

Figure 25: The variation of Altitude and Velocity

Second Iteration

For the second iteration IAD shape and design the variation of Altitude and Velocity is shown in Fig. 26. This corresponds to the variation of Cd as shown in Fig. 15

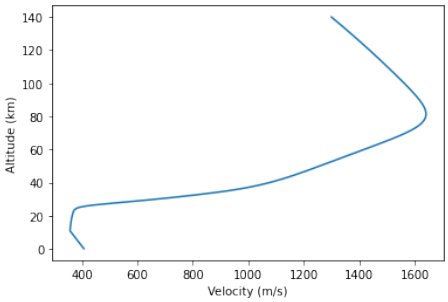

Figure 26: the variation of Altitude and Velocity

In both these iterations the lowest velocity achievable is 400m/s. This value must be reduced further so that smooth and proper landing can take place. For this the IAD shape has to be further optimized. If all the velocity can't be killed by the IAD, even for the parachutes to be able to do it we need the velocity to be around at least 160m/s. One other option can be to use retro propellants used during separation to reduce velocity but due to this more mass would be added to the system leading to payload penalty.

The representational image of the fully deployed IAD and Grid Fins that we intend to design is shown in Fig. 27

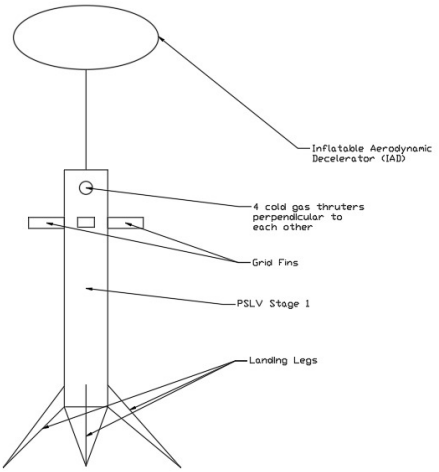

Figure 27: Representational Image of the system

The trajectory and sequence of events for the system are shown in the Fig. 28 according to our initial idea where IAD is sufficient to provide enough deceleration. If that is not possible additional parachutes would be required.

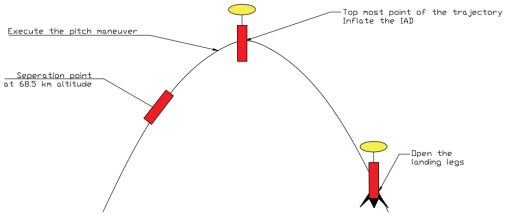

Figure 28: Sequence of Events

Conclusions

Based on the studies that could be conducted within the time frame of the project, the following observations and conclusions can be made,

1. The velocity at touchdown for the initial two simulations is around 400 m/s and this is very high and at present the chances of successful design of an IAD for recovery of PS1 seems slim.

2. IAD shape optimizations can be conducted further to improve the touchdown velocity. The maximum Cd we have obtained is in the second iteration with Cd about 1. This happens at a mach number of about 1.75. Optimizations must be done in the direction shifting the peak towards the Mach numbers which occur during major parts of the flight.

3. We can also explore the options of using a retro thruster at around 20 km to reduce the velocity further but this would increase the mass of the system.

4. Due to structural stability we can not vary geometry parameters beyond a particular limit.

5. Even if we can achieve lower velocities say in the range 100m/s which would necessitate the use of parachutes, given the mass of the PS1 stage at least 3 parachutes would be required. The mass estimate of the parachute is about 147 kg.

6. Also Addition of Parachutes along with IAD can complicate the system and the total integration can pose serious problems as the IAD is itself trailing.

7. The mass estimate for the Landing legs itself is around 475 kg. The Average payload capacity for PSLV is 1500kg. Thus we will have a maximum payload penalty component of about $\frac{475}{40}$ kg from the Landing legs.

8. Considering the above facts encountered during the course of our project we are sure that there will be payload penalties and also complexities in the integration if both IAD and parachutes are required. Not only the mass penalty the highly optimized PSLV performance will also get affected due to changes in this. Hence another option can be, which is the case for current launch vehicles that exhibit reusability , is to design a new launch vehicle keeping in mind the reusablility.

9. The main drawback for the PS1 stage is its mass as IAD concept has proven successful for sounding rockets and other lighter structures.

Acknowledgements

We would like to thank Dr. Ayyappan G (VSSC, ISRO) and Dr. Manoj T Nair (IIST, ISRO) for their continuous guidance and support both technical and non-technical during the project and also for providing this project for the course. We would also like to thank Dr.Pankaj Priyadarshi (VSSC, ISRO), Ankita Hudedagaddi A&M (STS, VSSC) and alumni of IIST for their guidance for the project.

References

[1] Development of a Cold Gas Propulsion System for the TALARIS Hopper, Sarah L. Nothnagel, 2011

[2] Moonan, William C., "Evaluation of the Aerodynamics of an Aircraft Fuselage Pod Using Analytical, CFD, and Flight Testing Techniques. " Master's Thesis, University of Tennessee, 2010. https://trace.tennessee.edu/utk_gradthes/823

[3] FirstPost NS, Union Budget 2021, DoS granted funds. https://www.firstpost.com/india/union-budget-2021-mission-9264471.html

[4] http://arc.aiaa.org DOI: 10.2514/6.2013-1389

[5] PSLV C1 - IRS 1D Mission

[6] DESIGN OF A GRID FIN AERODYNAMIC CONTROL DEVICE FOR TRANSONIC FLIGHT REGIME, ERDEM DIKBAS

[7] http://arc.aiaa.org DOI: 10.2514/6.2014-1092 Supersonic Inflatable Aerodynamic Decelerators for use on Sounding Rocket Payloads

[8] ISRO'S SOLID ROCKET MOTORSt R. NAGAPPA, M. R. KURUP and A. E. MUTHUNAYAGAM, Acta Astronautica Vol. 19, No. 8, pp. 681 97, 1989

[9] https://www.moog.com/content/dam/moog/literature/Space_Defense/spaceliterature/propulsion/moog-coldgasthrusters-datasheet.pdf

[10] https://www.moog.com/content/dam/moog/literature/Space_Defense/spaceliterature/propulsion/Moog-MonopropellantThrusters-Datasheet.pdf

[11] MORPHING HYPERSONIC INFLATABLE AERODYNAMIC DECELERATOR, https://arc.aiaa.org/doi/abs/10.2514/6.2013-1256

[12] Supersonic Inflatable Aerodynamic Decelerators for use on Sounding Rocket Payloads, Matthew J. Miller, Bradley A. Steinfeldt, Robert D. Braun, (2014), AIAA Atmospheric Flight Mechanics Conference

[13] Design and dynamic analysis of landing gear system in vertical takeoff and vertical landing reusable launch vehicle, Ming ZhangDafu, XuShuai, YueShuai, YueHaifeng Tao, journal of aerospace engineering.

[14] Optimization design containing dimension and buffer parameters of landing legs for reusable landing vehicle, Bo LEI a, Ming ZHANG a,Hanyu LIN a, Hong NIE b, Chinese Society of Aeronautics and Astronautics and Beihang University, Chinese Journal of Aeronautics.

[15] Liquid spring damper for vertical landing Reusable Launch Vehicle under impact conditions Shuai Yue a,Branislav Titurus b, Hong Nie a,Ming Zhang a, Mechanical systems and signal processing, elsevier.

[16] Design and Selection Criteria of Main Parachute for Re-entry Space Payload Mahendra Pratap#,*, A.K. Agrawal@, and Swadesh Kumar#,Defence Science Journal, Vol. 69, No. 6, November 2019, pp. 531-537, DOI : 10.14429/dsj.69.12681

[17] W. Mueller: "Parachutes for Aircraft". National Advisory Committee for Aeronautics, NACA TM-450, October 1927.